# Coupling light into a guided Bloch surface wave using an inversely designed nanophotonic cavity

# Coupling light into a guided Bloch surface wave using an inversely designed nanophotonic cavity

Zongyuan Tang*,[1,2] Tian-Long Guo*,[3] Yannick Augenstein,[4,5] Adriano Troia,[6] Yanjun Liu,[2] Matthieu Roussey,[3] Carsten Rockstuhl,[4,7] and Emiliano Descrovi[1]

[1)] *Dept. of Applied Science and Technology, Politecnico di Torino, 10129 Torino, Italy*

[2)] *Dept. of Electronic and Electrical Engineering, Southern University of Science and Technology, 518055 Shenzhen, China*

[3)] *Center for Photonics Sciences, University of Eastern Finland, P.O. Box 111, FI-80101 Joensuu, Finland*

[4)] *Institute of Theoretical Solid State Physics, Karlsruhe Institute of Technology, 76131 Karlsruhe, Germany*

[5)] *Flexcompute Inc, 130 Trapelo Rd., Belmont, Massachusetts 02478, USA*

[6)] *Istituto Nazionale di Ricerca Metrologica (INRiM), 10135 Torino, Italy*

[7)] *Institute of Nanotechnology, Karlsruhe Institute of Technology, 76131 Karlsruhe, Germany*

(*Authors to whom correspondence should be addressed: Z. Tang, zongyuan.tang@polito.it; T.-L. Guo, tianlong.guo@uef.fi)

Controlling the propagation of light in the form of surface modes on miniaturized platforms is crucial for multiple applications. For dielectric multilayers that sustain Bloch surface waves at their interface to an isotropic dielectric medium, a conventional approach to manipulate them exploits shallow surface topographies fabricated on top of the truncated stack. However, such structures typically exhibit low index contrasts, making it challenging to confine, steer, and guide the Bloch surface waves. Here, we theoretically and experimentally demonstrate a device for a Bloch surface wave platform that resonantly couples light from a cavity to a straight waveguide. The structure is designed using topology optimization in a 2D geometry under the effective index approximation. In particular, the cavity-waveguide coupling efficiency of the radiation emitted by an individual source in the cavity center is optimized. The cavity is experimentally found to exhibit a narrow resonant peak that can be tuned by scaling the structure. The waveguide is shown to guide only light that resonates in the cavity. Fully three-dimensional simulations of the entire device validate the experimental observations.

Light manipulation in the form of surface electromagnetic waves[1] on a chip has long been recognized as an enabling technology for many applications, from sensing to integrated photonics. Among various families of surface electromagnetic waves, Bloch surface waves (BSWs) at the interface between dielectric multilayers and a dielectric medium have attracted considerable interest. When compared, e.g., to propagating surface plasmon polaritons, BSWs are distinct as they can be sustained across a broad wavelength range[2–4] at both polarizations[5,6]. BSWs are characterized by extremely long propagation lengths thanks to a vanishing intrinsic dissipation[7] and offer emission enhancement capabilities from nearby quantum emitters with no or little quenching[8]. Altogether, BSWs constitute a versatile platform, also because their dispersion in momentum and energy space can be engineered to carefully control the spatial extension of the associated evanescent fields extending in the outer media and the propagation constant, so in essence, the effective index[9].

To steer the propagation of BSWs on a surface, multilayers can be coated with a spatially structured thin dielectric layer. In doing so, a spatially dependent refractive index is introduced, which controls the BSW propagation thanks to a dielectric loading mechanism.[10–14] Fundamental optical components such as lenses can be implemented[15] using basic index profiles. However, a substantial change in the effective index of the BSW is not possible, index variations in the order of $\approx 0.1$ being typically reached. Therefore, to effectively steer light on the chip, non-intuitive designs should be conducted to enable a desired functionality. The design of these elements essentially constitutes an inverse problem. In the past, elements to control light propagation have been demonstrated, e.g., to focus an incident BSW into a predefined spot.[16]

Whereas the efficient control of BSWs is one crucial aspect, it remains an open question of how a supporting photonic structure could look like for effectively extracting light from an emitter and funneling it into a BSW mode. Placing an emitter on the flat surface and extracting the emitted BSW-coupled radiation is convenient for some applications[17], but it may exhibit sub-optimal efficiency. In addition, BSWs are characterized by modest Purcell factors, mainly because of the large associated mode volume. To overcome such a limitation, we propose here a resonant cavity for TE-polarized BSWs connected to a ridge waveguide. The cavity maximizes the amount of light injected into the waveguide from a dipolar emitter in the cavity center. The structure has been designed by topology optimization,[18] which aims to find an optimal structure for a well-defined object function. Here we report on the implementation of such a concept, showing that the cavity-waveguide system is effective in injecting narrowband guided BSW from the cavity upon external illumination in proper conditions.

A basic sketch of the device can be seen in Fig. 1(a). It consists of the multilayer stack (BSW platform) and a free-form cavity connected to a waveguide on the topmost layer. The cavity and the waveguide are defined by structuring the topmost layer in the *xy*-plane. The multilayer (or 1D photonic crystal, 1DPC) consists of a stack of alternating $TiO_2$ and $SiO_2$ layers on a glass coverslip, topped by an $Al_2O_3$ etch-stop layer and a $SiO_2$ layer wherein cavity and waveguide are etched. Patterning this last layer encodes the desired optical

functionalities. The entire stack has the following structure, starting from the glass substrate: ($TiO_2$ - $SiO_2$)×3 - $TiO_2$ - $SiO_2$ - $Al_2O_3$ - $SiO_2$, with corresponding layer thicknesses: (80 nm - 105 nm)×3 - 80 nm - 125 nm - 25 nm - 60 nm. In the following, the 1DPC without the top $SiO_2$ layer will be referred to as "bare", in contrast to the "coated" 1DPC, which includes all layers listed above. The 1DPC deposition was performed as detailed in the Supplementary Information.

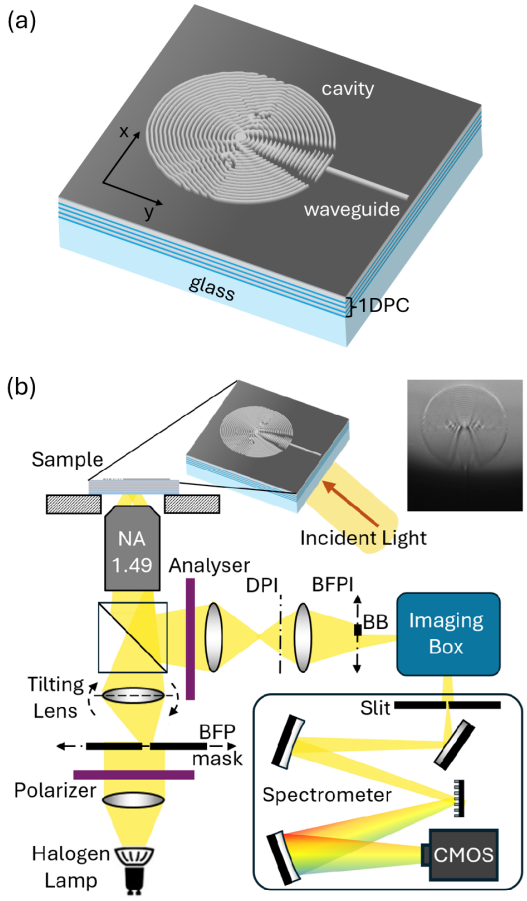


FIG. 1. (a) Sketch of an illustrative cavity and waveguide structure etched on top $SiO_2$ of the dielectric multilayer; (b) sketch of the experimental setup based on a customized inverted microscope coupled with a spectrometer. A halogen lamp provides illumination. BB: beam-blocker; DPI: Direct Plane Image; BFPI: Back Focal Plane Image.

Designing resonant elements on a BSW platform requires knowledge on the BSW dispersion,[19–22] which is deduced from reflectivity measurements performed on a customized setup based on an inverted microscope. According to the setup sketch in Fig. 1(b), white-light radiation from a halogen lamp is expanded, spatially filtered by a holed opaque mask, and then focused onto the entrance pupil of an oil-immersion objective (NA=1.49). The focusing lens can be tilted with respect to the optical axis and is configured so that the mask is projected onto the back focal plane (BFP) of the objective. The BFP mask can be laterally translated relative to the optical axis. With this precaution, the illumination spot can be directed onto the sample plane at arbitrary incidence angles and positions within the field of view, a crucial step to control BSW coupling. In addition, the illumination light can be polarized through a polarization filter. The oil-immersion objective collects reflected and leakage radiation that are polarization-filtered using a rotating analyzer. Direct plane image (DPI) and back focal plane image (BFPI) are formed by a pair of lenses, as indicated in the sketch. Access to these intermediate images allows us to perform further spatial/Fourier filtering. In particular, a movable beam blocker on the BFPI can filter out a significant part of the reflected light, facilitating the detection of the leakage radiation, which ultimately carries information about the BSW spatial distribution[23,24]. An imaging box allows us to alternatively project either the DPI or the BFPI onto the entrance slit of a spectrometer. The slit is placed vertically and aligned along the DPI dimension parallel to the *y*-axis in Fig. 1(a). It allows us to select the portion of the image (either DPI or BFPI) for the spectral analysis. A 600 lines/mm blazed grating is employed within a 300 mm-focal length spectrometer. In standard imaging mode, the dispersion grating is operated as a mirror ($0^{th}$ order of diffraction). In contrast, in spectroscopic imaging mode, the $1^{st}$ order of diffraction is exploited instead. When the BFP is imaged in spectroscopic mode, one dimension of the image is related to wavelengths and the other to the effective index along the y-axis direction.[25]

In Fig. 2, s-polarized reflection maps of a flat "bare" 1DPC are shown as collected in spectroscopic BFP imaging mode. Three separate spectral domains ranging from $\lambda$=480 nm to $\lambda$=640 nm are reported. The sharp reflectivity change at $n_{eff} = 1$ indicates the condition of total internal reflection (TIR). The TE-polarized BSW dispersion emerges as a reflectivity dip beyond the critical angle. We found an excellent agreement with the BSW dispersion curve calculated through a standard transfer matrix method (dashed black line).[26] Taking in mind that TE-polarized modes can be mapped when s-polarized light is detected, it is worth mentioning that the BSW dip disappears when the polarization analyzer is rotated by 90°, allowing p-polarized light only to be collected.

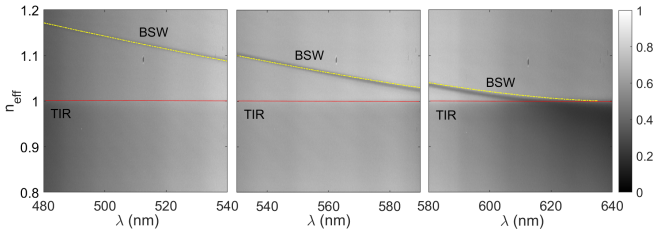


FIG. 2. s-polarized reflectivity maps R($\lambda$,$n_{eff}$) of the "bare" 1DPC collected in spectroscopic BFP imaging configuration. BSW is visible as a reflectivity dip. The calculated BSW dispersion is also shown (dashed yellow line). Total Internal Reflection (TIR) occurs at $n_{eff} = 1$.

We perform a topology optimization in a simplified two-dimensional setting to optimize the cavity and design the entire device. Following our prior work,[18], we initially considered light propagation in the *xy*-plane plane corresponding to

the in-plane propagation of the BSW. The cavity consists of a circular domain with a diameter of 10.7 $\mu$m. Within that spatial region, the refractive index distribution can be optimized using topology optimization to inject the emission from an emitter in the center of the domain into a connected waveguide, whose width is 260 nm (Fig. 1(a)). All details on the optimization can be found in Ref.[18]. To compare the measured response presented below to simulations, we resort to a full-wave 3D simulation of the actual layer stack used in the measurements and perform adapted simulations to predict the measured observables. Fabrication is performed by following a process involving Electron Beam Lithography and etching steps, as described in the Supplementary Information.

In Fig. 3, exemplary images of the cavities are shown, as collected at the scanning electron microscope (SEM) and the optical microscope in bright field (BF) and dark field (DF) modes. In particular, the DF image gives an account of the scattered field (s-polarization) that recapitulates the complex topography of the cavity.

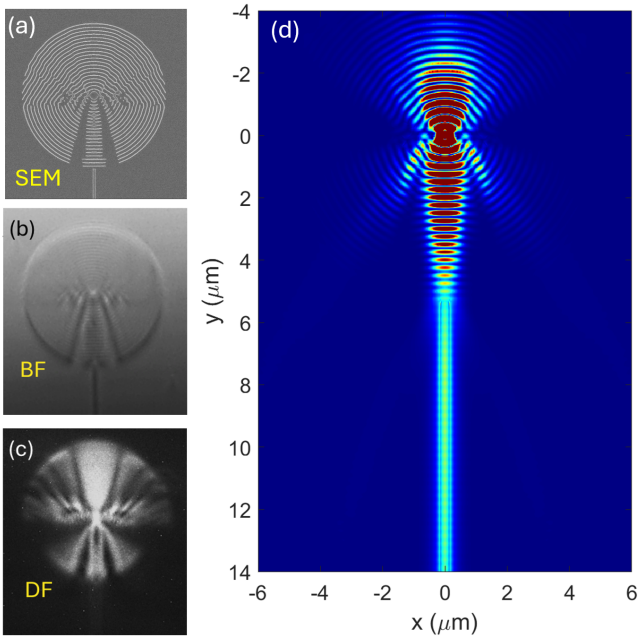


FIG. 3. Images of a fabricated cavity taken in the (a) Scanning Electron Microscopy and the optical microscope in (b) Bright Field and (c) Dark Field, respectively. The DF image is collected in a no-BSW coupling condition. (d) Intensity distribution ($|E(x,y)|^2$)) of light emitted by a dipole in the cavity center and coupled within the waveguide. The colormap is thresholded such that the intensity at the source location is at saturation.

As described above, the resonant cavity is designed to optimize the coupling from a single emitter located at its center. The electric dipole momentum was assumed to be in the 1DPC plane and perpendicular to the waveguide. In such a situation, the short distance between the emitter and the structure would substantially alter the emitter's radiative behavior in terms of decay rate (e.g., Purcell effect) and power spectrum in the momentum space. In particular, thanks to the high Local Density of States (LDOS) offered by the BSW on the 1DPC top surface, a significant amount of emitted power would be naturally transferred to the surface mode, resulting in the so-called Bloch surface wave coupled emission (BSWCE)[27,28]. This situation is clearly illustrated in Fig. 3(d), where the intensity distribution of light emitted by a dipolar source in the cavity center (i.e., $x = 0$ $\mu$m, $y = 0$ $\mu$m, $z = -h_{\mathrm{wvg}}/2$ with, $z = 0$ $\mu$m being the terminating interface of the entire structure) is calculated by a fully 3D FDTD model (Tidy3D). The discontinuity in the intensity distribution, specifically visible at the waveguide sidewalls, comes from the x-component of the shown electric field being discontinuous because of the usual interface conditions from the Maxwell equations (see Supplementary Figures S2, S3). The intensity is shown in the plane of the emitter. However, if the cavity is fed with far-field propagating radiation, as in the present case, coupling to BSW is generally poorly favored unless specific illumination conditions are met. For this reason, we control the illumination spot such that its incidence angle is above the critical angle (TIR condition), with the direct illumination hitting the cavity only while leaving the waveguide unilluminated (see top-right inset in Fig. 1(b)). In addition, to have a good separation between reflected and leakage radiation on the BFP and to facilitate the background filtering, the illumination direction is set as antiparallel to the $y$-axis so that any guided mode heading towards the waveguide end will be ascribed to back scattering from the cavity only, with a negligible contribution from direct illumination. With this arrangement, we facilitate the coupling of BSW in the cavity region and the collection of leakage radiation from guided BSWs.

The results of the optical characterizations are shown in Fig. 4. In Fig. 4(a), a DPI of the cavity and the waveguide is presented, wherein the reflected light is substantially filtered out by the beam blocker on the BFP, leaving scattered and leakage radiation only to reach the camera. Radiation injected into the waveguide and propagated through the waveguide is clearly visible. Worth underlining that the waveguide is not directly illuminated, and the illumination direction from the objective is antiparallel to the propagation direction of the guided BSW.

When the DPI is projected onto the spectrometer and the entrance slit is sufficiently narrow to select only a vertical strip centered about the waveguide, a wavelength-dispersed image of the $x = 0$ cross-section is obtained (Fig. 4(b)). The spectral signature of the guided BSW is substantially dominated by a 1.4 nm FWHM peak, centered at about $\lambda$ =565 nm, kept across the cavity center and the waveguide. This evidence suggests that light into the waveguide comes from a resonant scattering by the cavity, after BSW coupling from the external white-light illumination. The weak periodic modulation along the waveguide direction in Fig. 4(b) is probably caused by interference of the leakage radiation from guided BSW with a residual reflected light having comparable wavevectors.

The spatial confinement of guided modes in the transverse direction of the waveguide corresponds to a broad angular spectrum in the Fourier space, specifically in the wavevector component transverse to the propagation direction. This has been widely observed in, e.g., BSW waveguides[29–31], plasmonic[25,32], and hybrid guiding systems[33,34]. When the imag-

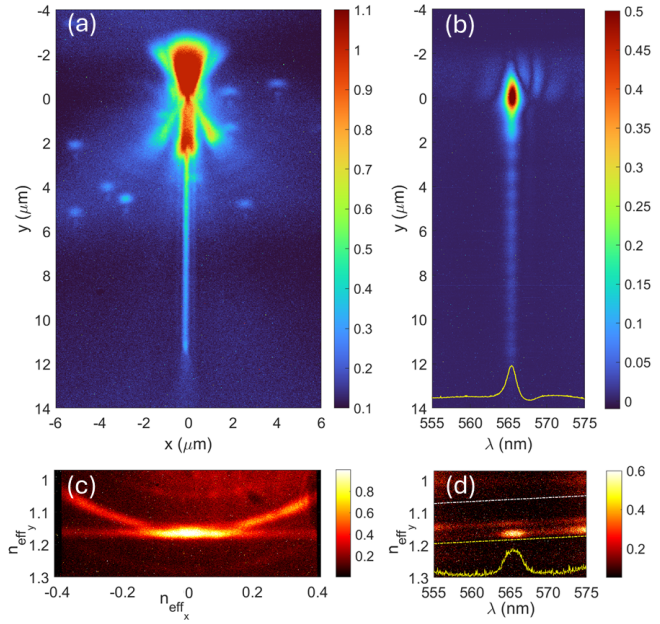


FIG. 4. (a) Full-spectrum DPI of the cavity and waveguide, after spatial filtering of the reflected light; (b) spectrally resolved DPI (normalized and background-subtracted) of the cavity and waveguide taken along the $x = 0$ cross-section in (a). The yellow line depicts the spectrum of the guided BSW, integrated along the whole waveguide length; (c) BFPI on the ($n_{eff_x}$, $n_{eff_y}$) plane corresponding to the image in (a), where only the lower BFPI portion with wavevectors parallel to the positive y-axis is visible; (d) spectrally-resolved BFPI along the $n_{eff_x} = 0$ cross-section in (c) showing the guided BSW mode dispersion. Calculated BSW dispersions on the "bare" 1DPC (white dash-dotted line) and "coated" 1DPC (black dash-dotted line) are also shown.

ing box is configured to project the BFPI onto the spectrometer, the intensity distribution shown in Fig. 4(c) is observed. In this pattern, we recognize a bright arc corresponding to the scattered BSW, propagating radially from the cavity and an additional straight line associated with the BSW-guided mode within the ridge. When the spectrometer slit is closed to select a vertical strip centered on the BFPI at $n_{eff_x} = 0$, the dispersion of the BSW guided mode can be retrieved. In Fig. 4(d), we observe a clear localization of light within a 3 nm-wide spectral interval, peaked at $\lambda$ =565 nm. The spectral shape is affected by the slit opening, which has been kept wider as compared to the case in Fig. 4(b) because of the need to collect stronger light signals onto the camera. Worth to note that the guided BSW has an effective index between the BSW dispersion on the "bare" 1DPC and the BSW dispersion on the "coated" 1DPC, i.e., $n_{eff}^{bare} < n_{eff}^{guided} < n_{eff}^{coated}$, where $n_{eff}^{bare} = 1.06$, $n_{eff}^{guided} = 1.165$ and $n_{eff}^{coated} = 1.18$. This is expected, as the guided mode confined within the ridge possesses evanescent tails extending transversely on both sides, thus decreasing the mode effective refractive index as compared to the cases of a uniform slab or very wide ridge. Thanks to the dielectric loading mechanism, increasing the ridge height leads to an increase of $n_{eff}^{coated}$, while increasing the ridge width makes the waveguide to become multimodal.[19,35]

Linear scaling of the optimized cavity pattern provides an additional way to fine-tune the spectral position of resonant modes. We upscaled the dimensions of the cavity described above by linear factors $\Delta l/l = 6\%, 18\%$, resulting in the redshifted spectra shown in Fig. 5(a). The waveguide width is kept unchanged. Also, resonance bandwidths are seen to increase as the peak wavelength increases. As the BSW dispersion approaches the light line at longer wavelengths, resulting in more extended evanescent tails, a lower effective index of the resonant modes and corresponding weaker confinement are produced. We could observe no guided/resonant mode peaks for larger scaling factors, probably because no BSWs are available anymore at wavelengths longer than 630 nm. This trend is also confirmed by FDTD simulations on the 3D model, wherein the dipolar emitter is placed in the cavity center, and the power flow out of the waveguide is monitored (Fig. 5(b)). Calculated resonant peaks are slightly redshifted with respect to measurements, such that the discrepancy increases with cavity size and peak wavelengths. This is not surprising, as small thickness variations in the deposited 1DPC layers can result in BSW shifts that ultimately affect the resonance spectral positions, in particular at longer wavelengths, where the BSW dispersion deviates from being linear when approaching the light line.

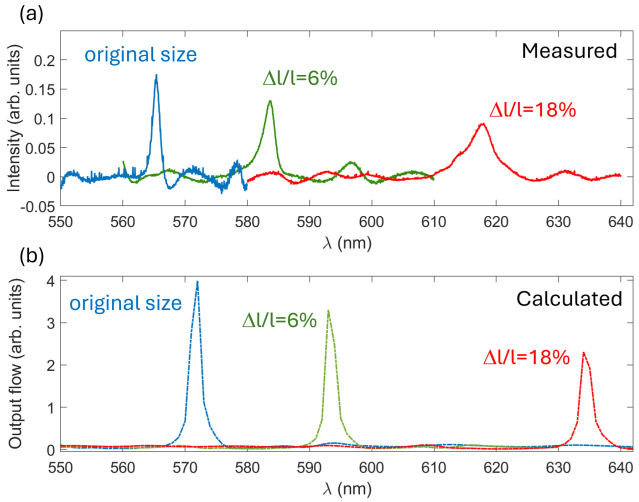


FIG. 5. (a) Measured transmission spectra of guided BSW from scaled cavities: original pattern (blue line); scaled cavity with $\Delta l/l = 6\%$ (green line), scaled cavity with $\Delta l/l = 18\%$ (red line); (b) Calculated output flow from the waveguide: original pattern (blue dashed line), scaled cavity with $\Delta l/l = 6\%$ (green dashed line), scaled cavity with $\Delta l/l = 18\%$ (red dashed line).

In conclusion, we provided experimental validation of an on-chip photonic component for BSW consisting of a resonant planar cavity coupled to a waveguide. The cavity design is obtained by exploiting a 2D topology optimization method to maximize the power injection from an isolated emitter into the waveguide. Characterization based on white light illumination shows a narrow resonant peak ($\Delta\lambda \simeq 1.4$ nm) that is propagated through the waveguide. By carefully acting on the linear size of the cavity pattern, the resonant peak can be

spectrally shifted, provided BSW modes are supported by the underlying multilayer. The system considered in this work is characterized by low effective refractive index contrast in a quasi-2D photonic environment wherein the cavity pattern is etched in a 60 nm thick $SiO_2$ layer. In perspective, these kinds of devices may represent interesting platforms for on-chip polaritonics[36–39], nano-lasers[40] and quantum nanophotonics, provided the deterministic integration of quantum sources such as colloidal quantum dots[41], molecules[42], or color centers[43].

## SUPPLEMENTARY MATERIAL

See the supplementary material for more details on the fabrication process, the cavity design based on topology optimization and the BSW propagation along the ridge waveguide.

## ACKNOWLEDGMENTS

Y.A. and C.R. acknowledge support from the German Research Foundation within the Excellence Cluster 3D Matter Made to Order (EXC 2082/1 under project number 390761711) and by the Carl Zeiss Foundation. The work received financial support through the project RAVEN from the European Union's Horizon Europe research and innovation programme under grant agreement number 101135787 and the Research Council of Finland Flagship PREIN (decision 346518).

## AUTHORS DECLARATIONS

### Conflict of interest

Y.A. has financial interest in Flexcompute Inc, which develops the software Tidy3D used in this work.

### Authors contributions

**Zongyuan Tang:** Validation (lead); Investigation (equal); Writing – original draft (lead); Writing-Review & Editing (equal); **Tian-Long Guo:** Methodology (lead); Investigation (equal); Resources (supporting); Writing-Review & Editing (equal); **Yannick Augenstein:** Formal Analysis (lead); Software (lead); Investigation (equal); Methodology (supporting); Writing-Review & Editing (equal); **Adriano Troia:** Resources (lead); Investigation (equal); Writing-Review & Editing (equal); **Yanjun Liu:** Funding Acquisition (lead); Investigation (equal); Writing-Review & Editing (equal); **Matthieu Roussey:** Project Administration (lead); Funding Acquisition (supporting); Investigation (equal); Writing-Review & Editing (equal); **Carsten Rockstuhl:** Conceptualization (lead); Investigation (equal); Supervision (supporting); Resources (supporting); Writing-Review & Editing (equal); **Emiliano Descrovi:** Supervision (lead); Investigation (equal); Writing – original draft (Supporting); Writing-Review & Editing (equal);

## DATA AVAILABILITY STATEMENT

The data that support the findings of this study are available from the corresponding author upon reasonable request.

## REFERENCES

[1] J. Polo Jr. and A. Lakhtakia, "Surface electromagnetic waves: A review," Laser & Photonics Reviews **5**, 234–246 (2011).
[2] G. M. Smolik, N. Descharmes, and H. P. Herzig, "Toward bloch surface wave-assisted spectroscopy in the mid-infrared region," ACS Photonics **5**, 1164–1170 (2018).
[3] A. Occhicone, R. Polito, F. Michelotti, M. Ortolani, L. Baldassarre, M. Pea, A. Sinibaldi, A. Notargiacomo, S. Cibella, F. Mattioli, P. Roy, J.-B. Brubach, P. Calvani, and A. Nucara, "Low-temperature stability and sensing performance of mid-infrared bloch surface waves on a one-dimensional photonic crystal," ACS Applied Materials & Interfaces **14**, 43853–43860 (2022).
[4] B. Kalas, K. Ferencz, A. Saftics, Z. Czigany, M. Fried, and P. Petrik, "Bloch surface waves biosensing in the ultraviolet wavelength range – bragg structure design for investigating protein adsorption by in situ kretschmann-raether ellipsometry," Applied Surface Science **536**, 147869 (2021).
[5] G. Pellegrini, M. Finazzi, M. Celebrano, L. Duò, and P. Biagioni, "Chiral surface waves for enhanced circular dichroism," Physical Review B **95**, 1–5 (2017).
[6] M. Gryga, D. Ciprian, L. Gembalova, and P. Hlubina, en"Sensing based on Bloch surface wave and self-referenced guided mode resonances employing a one-dimensional photonic crystal," Optics Express **29**, 12996 (2021).
[7] B. Vosoughi Lahijani, N. Descharmes, R. Barbey, G. D. Osowiecki, V. J. Wittwer, O. Razskazovskaya, T. Südmeyer, and H. P. Herzig, "Centimeter-scale propagation of optical surface waves at visible wavelengths," Advanced Optical Materials **10**, 2102854 (2022).
[8] F. Michelotti and E. Sepe, "Anisotropic fluorescence emission and photobleaching at the surface of one-dimensional photonic crystals sustaining bloch surface waves. i. theory," The Journal of Physical Chemistry C **123**, 21167–21175 (2019).
[9] V. N. Konopsky and E. V. Alieva, "Photonic crystal surface waves for optical biosensors," Analytical Chemistry **79**, 4729–4735 (2007).
[10] L. Yu, E. Barakat, T. Sfez, L. Hvozdara, J. Di Francesco, and H. Peter Herzig, "Manipulating Bloch surface waves in 2D: a platform concept-based flat lens," Light: Science & Applications **3**, e124–e124 (2014).
[11] R. Wang, J. Chen, Y. Xiang, Y. Kuai, P. Wang, H. Ming, J. R. Lakowicz, and D. Zhang, "Two-Dimensional Photonic Devices based on Bloch Surface Waves with One-Dimensional Grooves," Physical Review Applied **10**, 024032 (2018).
[12] K. R. Safronov, D. N. Gulkin, I. M. Antropov, K. A. Abrashitova, V. O. Bessonov, and A. A. Fedyanin, "Multimode Interference of Bloch Surface Electromagnetic Waves," ACS Nano **14**, 10428–10437 (2020).
[13] X. Tang, H. Luo, J. Chen, R. Badugu, P. Wang, J. R. Lakowicz, and D. Zhang, "Converting the guided-modes of Bloch surface waves with surface pattern," J. Opt. Soc. Am. B **38**, 1579–1585 (2021).
[14] H. Luo, X. Tang, Y. Lu, and P. Wang, "Low-loss photonic integrated elements based on bound bloch surface wave in the continuum," Phys. Rev. Appl. **16**, 014064 (2021).
[15] M.-S. Kim, B. Vosoughi Lahijani, N. Descharmes, J. Straubel, F. Negredo, C. Rockstuhl, M. Häyrinen, M. Kuittinen, M. Roussey, and H. P. Herzig, "Subwavelength focusing of bloch surface waves," ACS Photonics **4**, 1477–1483 (2017).

[16] Y. Augenstein, A. Vetter, B. V. Lahijani, H. P. Herzig, C. Rockstuhl, and M.-S. Kim, "Inverse photonic design of functional elements that focus Bloch surface waves," Light: Science & Applications **7**, 104 (2018).

[17] A. Occhicone, F. Michelotti, P. Rosa, D. Chiappetta, T. Pileri, P. Del Porto, N. Danz, P. Munzert, G. Pignataro, and A. Sinibaldi, "Enhanced fluorescence detection of mirna by means of bloch surface wave-based biochips," Analyst **148**, 4429–4437 (2023).

[18] Y. Augenstein, M. Roussey, T. Grosjean, E. Descrovi, and C. Rockstuhl, "Inverse design of cavities for bloch surface waves interfaced to integrated waveguides," Photonics and Nanostructures - Fundamentals and Applications **52**, 101079 (2022).

[19] T. Perani, D. Aurelio, and M. Liscidini, "Bloch-surface-wave photonic crystal nanobeam cavity," Opt. Lett. **44**, 5133–5136 (2019).

[20] U. Stella, L. Boarino, N. D. Leo, P. Munzert, and E. Descrovi, "Enhanced directional light emission assisted by resonant bloch surface waves in circular cavities," ACS Photon. **6**, 2073–2082 (2019).

[21] N. Marcucci, M. C. Giordano, G. Zambito, A. Troia, F. B. de Mongeot, and E. Descrovi, "Spectral tuning of bloch surface wave resonances by light-controlled optical anisotropy," Nanophotonics **12**, 1091–1104 (2023).

[22] N. Marcucci, T.-L. Guo, S. Pélisset, M. Roussey, T. Grosjean, and E. Descrovi, "Bloch surface waves in open fabry–perot microcavities," Micromachines **14** (2023).

[23] J. Grandidier, G. C. des Francs, S. Massenot, A. Bouhelier, L. Markey, J.-C. Weeber, and A. Dereux, "Leakage radiation microscopy of surface plasmon coupled emission: investigation of gain-assisted propagation in an integrated plasmonic waveguide," Journal of Microscopy **239**, 167–172 (2010).

[24] E. Descrovi, E. Barakat, A. Angelini, P. Munzert, N. D. Leo, L. Boarino, F. Giorgis, and H. P. Herzig, "Leakage radiation interference microscopy," Opt. Lett. **38**, 3374–3376 (2013).

[25] S. Cueff, L. Berguiga, and H. S. Nguyen, "Fourier imaging for nanophotonics," Nanophotonics **13**, 841–858 (2024).

[26] J. Chilwell and I. Hodgkinson, "Thin-films field-transfer matrix theory of planar multilayer waveguides and reflection from prism-loaded waveguides," J. Opt. Soc. Am. A **1**, 742–753 (1984).

[27] M. Liscidini, M. Galli, M. Shi, G. Dacarro, M. Patrini, D. Bajoni, and J. E. Sipe, "Strong modification of light emission from a dye monolayer via bloch surface waves," Opt. Lett. **34**, 2318–2320 (2009).

[28] M. Ballarini, F. Frascella, N. D. Leo, S. Ricciardi, P. Rivolo, P. Mandracci, E. Enrico, F. Giorgis, F. Michelotti, and E. Descrovi, "A polymer-based functional pattern on one-dimensional photonic crystals for photon sorting of fluorescence radiation," Opt. Express **20**, 6703–6711 (2012).

[29] M. Ballarini, F. Frascella, E. Enrico, P. Mandracci, N. De Leo, F. Michelotti, F. Giorgis, and E. Descrovi, "Bloch surface waves-controlled fluorescence emission: Coupling into nanometer-sized polymeric waveguides," Appl. Phys. Lett. **100**, 063305 (2012).

[30] R. Wang, H. Xia, D. Zhang, J. Chen, L. Zhu, Y. Wang, E. Yang, T. Zang, X. Wen, G. Zou, P. Wang, H. Ming, R. Badugu, and J. R. Lakowicz, "Bloch surface waves confined in one dimension with a single polymeric nanofibre," Nature Communications **8**, 14330 (2017).

[31] T. Perani and M. Liscidini, "Long-range bloch surface waves in photonic crystal ridges," Opt. Lett. **45**, 6534–6537 (2020).

[32] J. Grandidier, S. Massenot, G. C. des Francs, A. Bouhelier, J.-C. Weeber, L. Markey, A. Dereux, J. Renger, M. U. González, and R. Quidant, "Dielectric-loaded surface plasmon polariton waveguides: Figures of merit and mode characterization by image and fourier plane leakage microscopy," Phys. Rev. B **78**, 245419 (2008).

[33] S. Frisbie, C. Regan, A. Krishnan, C. Chesnutt, J. Ajimo, A. Bernussi, and L. Grave de Peralta, "Characterization of polarization states of surface plasmon polariton modes by fourier-plane leakage microscopy," Optics Communications **283**, 5255–5260 (2010).

[34] D. G. Zhang, X.-C. Yuan, A. Bouhelier, P. Wang, and H. Ming, "Excitation of surface plasmon polaritons guided mode by rhodamine b molecules doped in a pmma stripe," Opt. Lett. **35**, 408–410 (2010).

[35] T. Sfez, E. Descrovi, L. Yu, D. Brunazzo, M. Quaglio, L. Dominici, W. Nakagawa, F. Michelotti, F. Giorgis, O. J. F. Martin, and H. P. Herzig, "Bloch surface waves in ultrathin waveguides: near-field investigation of mode polarization and propagation," J. Opt. Soc. Am. B **27**, 1617–1625 (2010).

[36] G. Lerario, A. Cannavale, D. Ballarini, L. Dominici, M. D. Giorgi, M. Liscidini, D. Gerace, D. Sanvitto, and G. Gigli, "Room temperature bloch surface wave polaritons," Opt. Lett. **39**, 2068–2071 (2014).

[37] G. Lerario, D. Ballarini, A. Fieramosca, A. Cannavale, A. Genco, F. Mangione, S. Gambino, L. Dominici, M. De Giorgi, G. Gigli, and D. Sanvitto, "High-speed flow of interacting organic polaritons," Light: Science & Applications **6**, e16212–e16212 (2017).

[38] B. Liu, J. Horowitz, and S. R. Forrest, "Guided bloch surface wave polaritons on patterned distributed bragg reflectors at room temperature," ACS Photonics **10**, 4476–4482 (2023).

[39] E. Maggiolini, L. Polimeno, F. Todisco, A. Di Renzo, B. Han, M. De Giorgi, V. Ardizzone, C. Schneider, R. Mastria, A. Cannavale, M. Pugliese, L. De Marco, A. Rizzo, V. Maiorano, G. Gigli, D. Gerace, D. Sanvitto, and D. Ballarini, "Strongly enhanced light–matter coupling of monolayer ws2 from a bound state in the continuum," Nature Materials **22**, 964–969 (2023).

[40] Y.-C. Lee, Y.-L. Ho, B.-W. Lin, M.-H. Chen, D. Xing, H. Daiguji, and J.-J. Delaunay, "High-q lasing via all-dielectric bloch-surface-wave platform," Nat. Commun. **14**, 6458 (2023).

[41] K. Ray, R. Badugu, and J. R. Lakowicz, "Bloch surface wave-coupled emission from quantum dots by ensemble and single molecule spectroscopy," RSC Adv. **5**, 54403–54411 (2015).

[42] P. Lombardi, A. P. Ovvyan, S. Pazzagli, G. Mazzamuto, G. Kewes, O. Neitzke, N. Gruhler, O. Benson, W. H. P. Pernice, F. S. Cataliotti, and C. Toninelli, "Photostable Molecules on Chip: Integrated Sources of Nonclassical Light," ACS Photonics **5**, 126–132 (2018).

[43] C. Wu, S. Kumar, Y. Kan, D. Komisar, Z. Wang, S. I. Bozhevolnyi, and F. Ding, "Room-temperature on-chip orbital angular momentum single-photon sources," Science Advances **8**, eabk3075 (2022).